Journal of Fluid Science and Technology

Vol. 5, No. 3, 2010

Universality of Longitudinal Vortices Shedding from a Cruciform Two Circular Cylinder System in Uniform Flow*

Tuananh NGUYEN**, Mizuyasu KOIDE***, Tsutomu TAKAHASHI** and Masataka SHIRAKASHI**

** Department of Mechanical Engineering, Nagaoka University of Technology, 1603-1 Kamitomioka, Nagaoka, Niigata, Japan.
E-mail:anhnt@stn.nagaokaut.ac.jp

*** Faculty of Economics, Niigata Sangyo University, Karuigawa 4730, Kashiwazaki, Niigata, Japan

Abstract

Earlier wind tunnel experiments supported by visualization in water flow carried out by the present authors showed that two types of longitudinal vortices shed periodically from a cruciform two identical circular cylinder system in uniform flow. These longitudinal vortices induce resonance-like oscillations over a wide velocity range accompanied by the synchronization phenomenon. The specific aim of this work is to investigate the universality of the longitudinal vortex shedding by carrying out experiments in both water and air flows. In addition to the velocity, the alternating lift force loading on the upstream cylinder in water flow is measured by using load-cells. The two longitudinal vortices are confirmed to shed periodically for small size systems in water flow in spite of large difference in the experimental conditions. Relationships of the Strouhal number and the lift force coefficient for the vortex shedding against Reynolds number agree well with the previous data except for the peculiar vanishing of the necklace vortex when Re is larger than 22000. The cause of this phenomenon is left for further investigation.

Key words: Periodical Vortex Shedding, Cruciform Cylinder System, Longitudinal Vortices, Trailing Vortex, Necklace Vortex

1. Introduction

The Karman vortex induced vibration (KVIV) of a cylinder in fluid flow is one of the most basic but still challenging subjects in the field of fluid engineering. Since this phenomenon has caused many serious accidents in mechanical engineering and structure engineering, numerous research works have been carried out so far to predict its behaviour and to avoid harmful oscillations induced by it [1]~ [5]. There are various methods to suppress KVIV such as suction holes on the surface of the body, tripping wires near the separation point, setting a splitter plate in the wake, and so on. In an earlier study carried out by the present authors as another approach, it was found that KVIV is effectively suppressed by setting another circular cylinder downstream with a proper gap in cruciform arrangement [6]. However, in the same arrangement, longitudinal vortices with rotation axes parallel to the free stream shed periodically and unexpected oscillations are caused in higher velocity ranges accompanied by the synchronization phenomenon (Lock-in) between the vortices and the cross-flow oscillation of the upstream cylinder [7], [8]. Type of the longitudinal vortex depends on the ratio of the gap s to the cylinder diameter d: (a) Trailing vortex when $0 \leq s/d \leq 0.25$ and (b) Necklace vortex when $0.25 \leq s/d \leq 0.5$ as shown in Fig.1 [9].

*Received 17 Sep., 2010 (No. 10-0419)
[DOI: 10.1299/jfst.5.603]

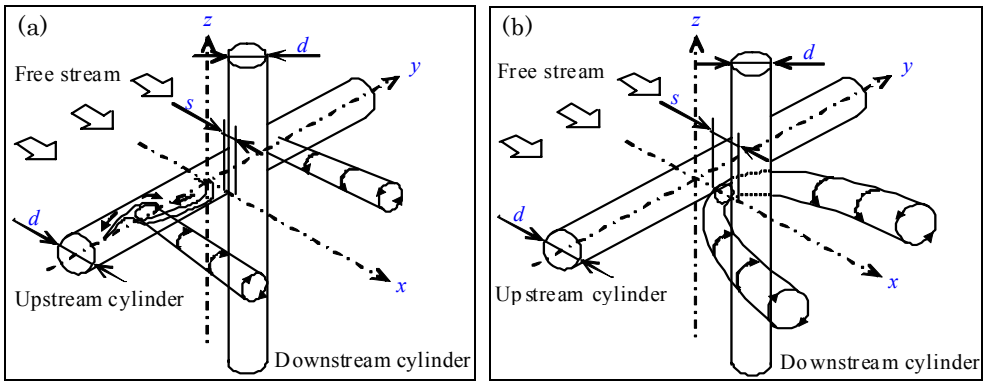

Fig.1 Longitudinal vortices shedding from cruciform cylinder system [9] (a) Trailing vortex, $0<s/d<0.25$; (b) Necklace vortex, $0.25<s/d<0.5$

While there are numerous studies on KVIV, studies on the longitudinal vortices are few and experiments on the longitudinal vortex induced vibration (LVIV) have been carried out under limited conditions. Zdravkovich [10] investigated the flow around two circular cylinders in contact forming a cross with two pairs of cylinders having diameters d = 25.4 mm and 50.8 mm and aspect ratios (the ratio of the cylinder length to the cylinder diameter) A_R = 18 and 9 respectively, in a wind tunnel with the test section of 0.45 m × 0.45m area. Fox [11], [12] investigated wake characteristics of fixed cruciform circular cylinder system with the size d = 16 mm and A_R = 20 in a low-velocity water tunnel having the test section of 1.63 m × 331.5 mm area. Den et al. (2006) carried out a numerical study about flow past a stationary circular cylinder and a downstream elastic circular cylinder in cruciform arrangement by using the virtual boundary method [13]. Shirakashi et al. [8] carried out experiments on the behavior of LVIV for system with cylinders d = 26 mm, A_R = 12.2 in a wind tunnel with the test section of 320 mm × 320 mm area. Koide et al. investigated universality of longitudinal vortex shedding from systems having around six time larger size by using a wind tunnel with the test section of 1800 mm × 1800 mm area [14]. More recently, we built a water tunnel with a 100 mm × 100 mm cross section to cover the velocity range up to U= 5 m/s to attain the Reynolds number range comparable with the above wind tunnel experiments. The results on the LVIVs obtained by the water tunnel showed that the trailing vortex induces vibrations in a similar way as in the air flow, but the vibration induced by the necklace vortex was unclear [15]. From the viewpoint of engineering, there is an urgent need to establish method to predict behaviour of the two LVIVs from cruciform systems with various sizes in both air and water flows and to avoid hazardous oscillations caused by this phenomenon. Hence, the specific aim of this study is to examine the universality of longitudinal vortices shedding from the cruciform system in the small-size water tunnel and comparing the results with various cylinder sizes in both air and water flows.

Nomenclature

A_R	aspect ratio (= l_e/d)
C_L	alternating lift coefficient ($C_L = F_L/0.5\rho U^2 d L_v$)
d	diameter of the cylinders
F_L	alternating lift exerting on the upstream cylinder
f_v	vortex shedding frequency
l_e	length of the cylinders, distance between the end plates (See Fig. 2)
L_v	span wise length of vortex shedding region
Re	Reynolds number (= $\rho dU/\mu$)
S_L, S_u	spectra of lift F_L and velocity u, respectively
St	Strouhal number for vortex shedding (= $f_v d/U$)

s gap between the two cylinders
U free flow velocity
u x-velocity component detected at a reference position
μ viscosity of fluid
ρ density of fluid

2. Experimental apparatus, measuring system and experimental conditions

2.1 Wind tunnels, water tunnels and cruciform circular cylinder systems

The cruciform system composed of two equal-diameter-circular-cylinders is fixed perpendicular to uniform flow as illustrated in Fig. 2, where the coordinate system used in this paper is also described.

In this paper, data for seven systems are compared with the experimental conditions given in Table 1. Among the seven systems, experiments in air flow were carried out for four systems: i.e. Systems I, II, III and IV, with cylinders of 26 - 127 mm diameters which were used in the previous work by the present authors [14]. Some data for Systems I, II in the wind tunnel A are also added, but for Systems III, IV in the wind tunnel B the same data presented in the previous paper are compared.

In this work, System I with the cylinder diameter d = 26 mm and the aspect ratio A_R = 12.2 is most widely examined so far for both rigidly and flexibly supported cases. System II with d = 45 mm was tested to investigate the influence of the aspect ratio and Systems III, IV for the cylinder size, on the longitudinal vortex shedding. System V with d = 22 mm was used for visualization in water flow.

Since the velocity range of the water tunnel A used for System V is limited as 0 ~ 0.5 m/s, another water tunnel which can attain ten times higher maximum velocity was built for Systems VI and VII with d = 10mm and 15mm respectively. Thus the experiments for these two systems covered a range of Reynolds number, Re, comparable with the case of System I. The aspect ratio of these two systems is a little lower than the wind tunnel experiments on Systems I, III and IV, and higher than or comparable with the system II.

2.2 Measurement of velocity, vortex shedding frequency and lift force

The free flow velocity, U, in wind tunnel A is measured by the ring-type velocimeter developed by the present authors [17]. For the two water tunnels, the free flow velocity was obtained from the flow rate. The relationship between the flow velocity U and the average velocity is obtained beforehand by applying the hydrogen bubble technique and the Pitot-tube-and-manometer instrument.

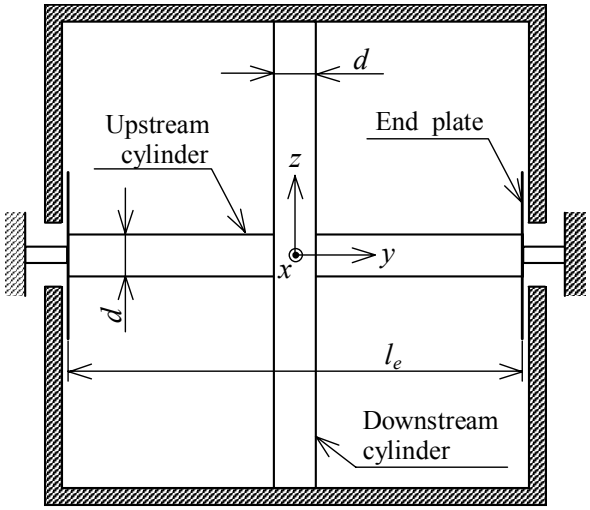

Fig. 2 Schematic diagram of cross section of a measuring section and coordinate system (viewed from downstream).

Table 1 Characteristics of cruciform circular cylinder systems in water and wind tunnels

System	Apparatus	Test section size [mm]	Velocity range [m/s]	Test cylinder			Reynolds number
				d [mm]	L [mm]	A_R	Re
I [8], [14]	Wind tunnel A	320× 320	1.5 ~ 40	26	318	12.2	3×10^3~4×10^4
II[14]				45	318	7.1	3.5×10^3~9×10^4
III[14]	Wind tunnel B	1800× 180 0	0 ~ 25	125	1800	14.4	5×10^3~9×10^4
IV[14]				127	1800	14.2	4.5×10^3~9×10^4
V	Water tunnel A	200× 200	0 ~ 0.5	22	200	9.1	0~5000
VI	Water tunnel B	100 × 100	0 ~ 5	10	100	10	3×10^3~4×10^4
VII				15	100	6.8	3×10^3~4×10^4

In the wind tunnel experiments, the vortex shedding frequency f_v is determined from the spectrum of velocity u, the x-component of the velocity fluctuation, detected by a hot wire probe. The probe positions appropriate for the necklace and the trailing vortices are decided to give the most definite peaks in the velocity spectrum S_u corresponding to their periodic shedding. In some cases of Wind tunnel A, a tuft grid is set downstream of the cruciform system to visualize the cross section of longitudinal vortices as seen in Fig.3. In this case the vortex shedding frequency f_v was obtained by counting the motion of the tufts in the slowly reproduced video image.

In the water tunnel experiments, a hot film probe was used instead of the hot wire probe to obtain the vortex shedding frequency f_v. The dye-streak injection technique was also applied in the water tunnel A to visualize the longitudinal vortices for the System V at low velocity. For the water tunnel B, the fluctuating lift force F_L loading on the upstream cylinder was measured by using a load cell, and f_v is also obtained from the spectrum of F_L.

3. Experimental results and discussions

3.1 Visualization of longitudinal vortices in air and water flows

Photographs in Fig. 3 present the cross section of the longitudinal vortices shedding in air flow for System II and the plan view in water flow for System V. In Fig.3 (a) a pair of vortices with opposite rotation symmetric about the vertical downstream cylinder is observed in the pattern of tufts corresponding to the pair of trailing vortices shown in Fig.1(a). This pattern appears periodically and alternately above and below the horizontal upstream cylinder. In Fig.3 (b) similar but less definite vortex patterns longer in span wise direction appear in the lower side of the upstream cylinder symmetric about the downstream cylinder. These express the cross section of curving part of the necklace vortex as seen in Fig.1 (b). Figs.3 (a') and (b') present the plan view of the trailing vortex and the necklace vortex respectively shedding from the cruciform systems in the water flow.

3.2 Vortex configuration dominated by gap-to-diameter ratio

Behavior of spectrum of velocity fluctuation S_u with increasing free stream velocity U for System VI are presented in Fig. 4. A sharp peak appears in a spectrum S_u at a frequency f_u which increases with flow velocity U for both cases of the gap-to-diameter ratio s/d = 0.08 and 0.28. These values of s/d are adopted here since the trailing and the necklace vortices are most clearly observed. Note that the positions of the hot film probe are adjusted so as to detect the velocity fluctuations corresponding with their periodical shedding. A lower peak which appears at a fixed frequency about 30 Hz for both two cases is caused by

noise signal. Hence, the definite peak at the frequency f_u is regarded as the shedding frequency f_v for the longitudinal vortices. While the sharp peak appears over the whole velocity range of measurement for the trailing vortex, s/d= 0.08, it seems to disappear or could not be clearly observed for the necklace vortex, s/d=0.28, as the velocity U exceeds about 1.6 m/s increasing gradient of f_u with U becomes lower, or even f_u seem to decrease. It is noted that this disappearance was not observed in the previous studies [14] for systems in air flow. Except this peculiar phenomenon, the results of the visualization shown in Fig.3 and the velocity spectra shown in Fig. 4 confirm that the trailing and the necklace vortices shed periodically in spite that the fluid, the cylinder diameter and aspect ratio are largely different from those of the earlier experiments.

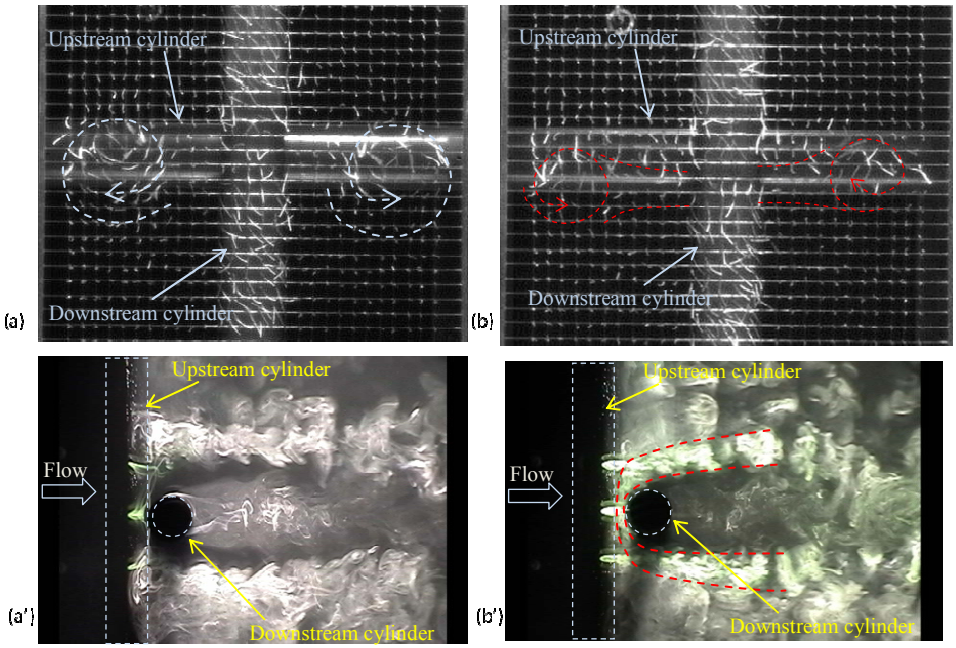

Fig.3 Photographs of visualized longitudinal vortices. Cross section by tuft grid observed from downstream for System II in air flow: (a) s/d = 0.08 at U = 5.4 m/s, grid position x/d = 1.9, f_v = 9.2 Hz, (b) s/d=0.28, U=5.5 m/s, x/d=2.1, f_v=6.3 Hz; Plan view for System V in water flow, U=0.1m/s, (a') s/d= 0.08, (b') s/d= 0.28.

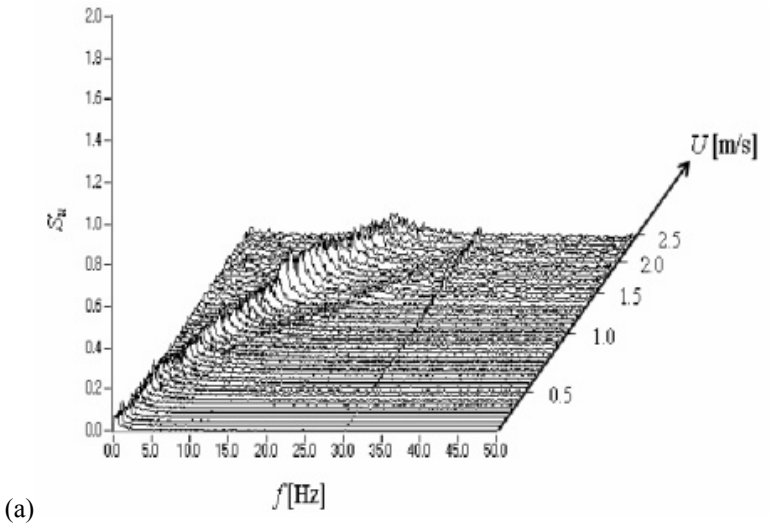

(a)

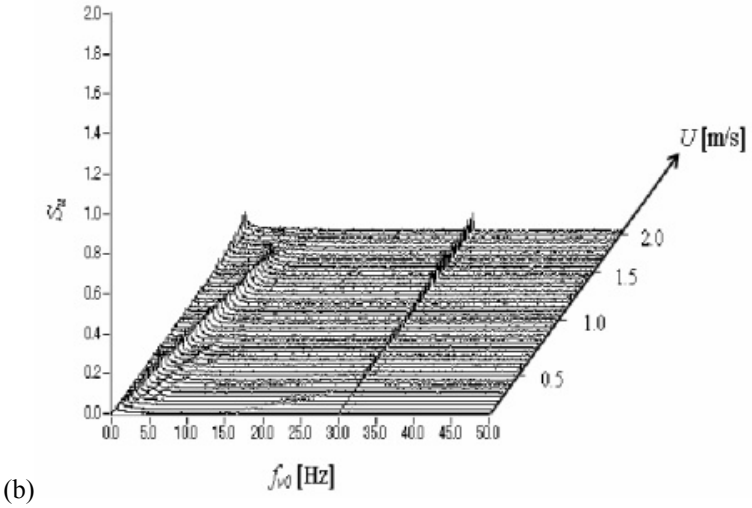

(b)

Fig.4 Velocity spectra S_u in the near wake of system VI. (a) s/d= 0.08; (b) s/d= 0.28

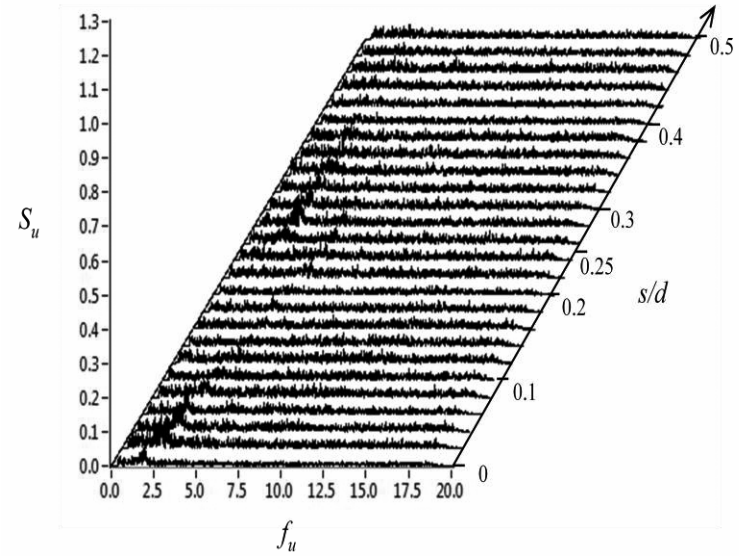

Fig.5 Spectra of velocity fluctuation S_u against s/d for System VII (d = 15 mm, U = 0.7 m/s, Re = 11000, probe position: x/d=1, y/d=1.25, z/d=0.25).

In order to see the transition from the trailing vortex to the necklace vortex, the velocity u was measured with the increasing gap-to-diameter ratio s/d while the free stream velocity U is kept constant. Figure 5 shows the velocity spectra S_u for the case of System VII (d = 15 mm) at Re=11000. When s/d < 0.25, a peak appears in S_u at a frequency f_u increasing slightly from 2.5 Hz to 5 Hz correspond to the trailing vortex. Then, the peak frequency f_u abruptly shifts to 3 Hz at $s/d \approx 0.25$, showing that the transition to the necklace vortex is occurring. It is noted that the spectrum peak corresponding to the trailing vortex shedding peak still appears when $0.25<s/d<0.3$ but its height is much lower than that for the necklace vortex. This denotes that both longitudinal vortices shed alternately at $0.25<s/d<0.3$ but the necklace vortex sheds much more regularly than the trailing vortex. This result of the transition between the two longitudinal vortices agrees well with data obtained for System I in the earlier study [8]. The necklace vortex peak in S_u in Fig.5 remains over the range of s/d up to 0.4.

The vortex shedding frequency $f_v=f_u$ is nondimensionalized into Strouhal number St defined by $f_v d/U$, and plotted against the gap-to-diameter ratio s/d for the various systems in Fig.6 (a), and the peak value of velocity spectrum S_u is also presented in Fig.6 (b).

(a)

(b)

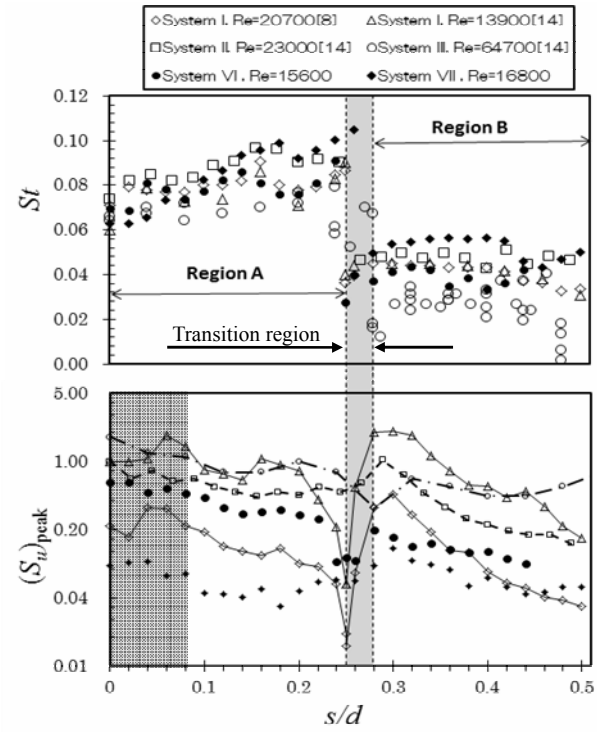

Fig.6 Strouhal number St and the peak value of velocity spectrum $(S_u)_{peak}$ versus the gap-to-diameter ratio s/d for various systems.

In Fig.6 (a), St ranges from 0.06 to 0.1 in Region A (s/d<0.25) corresponding to the trailing vortex shedding and shifts to less than 0.06 in Region B ($0.28<s/d<0.5$) corresponding to the necklace vortex shedding. The abrupt change in $(Su)_{peak}$ and St at $s/d \approx 0.25 \sim 0.28$ for Systems VI, VII at Re=15600 and 16800 agree well with the earlier experimental data [8], [14] at Re 13000 ~ 64700 obtained through larger size wind tunnel. However, the values of s/d for the transition and the upper limit for necklace vortex shedding do not so strictly agree among the systems, e.g. for System III with d=125 mm and A_R= 12 the behavior of $(S_u)_{peak}$ and St show that the transition point shifts to 0.28 and that the values of St are significantly lower than the others. This fact, together with Fig.5, shows that the transition occurs in the region s/d=0.25~0.28 indicated in the figure.

In the earlier works the values *s/d*= 0.08 and 0.28 were most frequently chosen as the typical cases of the trailing and the necklace vortex respectively for the systems I, II, III and V, VI. Fig.6 (b) shows that these two vortices were observed most definitely over ranges of *s/d* < 0.08 for the trailing vortex and 0.28 ~ 0.32 for the necklace vortex, as indicated in the figure.

The results in Fig. 6 confirm the universal nature of the trailing vortex shedding and the necklace vortex shedding depending on *s/d* and the transition between them in spite of the differences in fluids and in the cylinder diameter. The cause of significant deviation of the largest wind tunnel data from others in the vales of St and the transition *s/d* is unclear and left for further investigation.

3.3 Relation between Strouhal number and Reynolds number

In this section, we focus on the behavior of the longitudinal vortex shedding over a wide range of Reynolds number up to 10^5 for the systems in Table 1.

3.3.1 Trailing vortex

Figure 7 (a) shows the relationship between St and Re for the trailing vortex.

Except for Systems III and IV, results for the systems in Table 1 correlate well showing

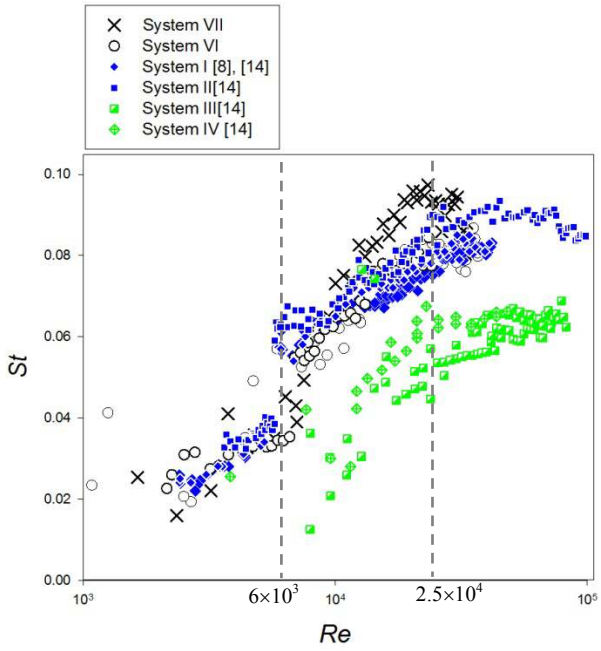

(a)

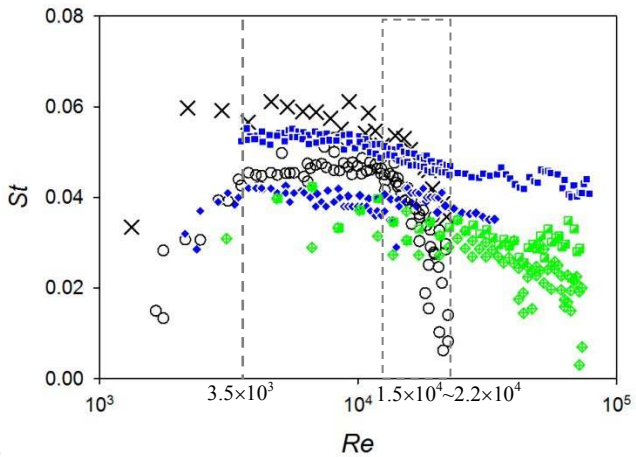

(b)

Fig.7. St vs. Re for various systems. (a): Trailing vortex, *s/d*=0.08; (b): Necklace vortex, *s/d*=0.28 or 0.3.

the following global feature. The St ~ Re curve is divided into three branches as indicated by the vertical broken lines. That is, in the range of $Re = 2\times10^3 \sim 6\times10^3$, Strouhal number St increases from 0.02 ~ 0.04 with Reynolds number Re. At $Re = 6\times10^3$ St suddenly jumps to 0.06, and continues to increase with the same gradient up to Re= 2.5×10^4 where St attains 0.08. Then St keeps a constant value of about 0.08 ~ 0.09 in the range of $2.5\times10^4 < Re < 10^5$. This behavior found in the previous study is confirmed again by the present work though experiments for systems VI and VII were carried out in the much smaller water tunnel. These results show the universal characteristics of the trailing vortex shedding.

In the case of systems III and IV (d = 125, 127 mm, $A_R \approx 14$) shown by green symbols in Fig.7 (a); the results show the similar tendency as in the above two higher Re ranges, that is, St increases with increasing Re and that approaches a certain constant value in the higher Re region. However, the value of St for these systems is 30 ~ 50 % lower than those for the other systems at the same Re and the constant value St reaches is about 0.06. The aspect ratio A_R (see Table 1) and the turbulence scale/intensity and end conditions are considered as potential causes of this discrepancy. However, sharp peaks in the velocity spectra S_u of these systems denote that the vortex shedding is regular and stable. On the other hand, there is no quantitative consistency in the influence of A_R because the data for systems I, II, VI, VII agree well together in spite of the difference in their aspect ratio. Hence the causes of discrepancy of St between two cases of systems are still unclear and left for further investigation.

3.3.2 Necklace vortex

Figure 7(b) shows the relationship between St and Re for the necklace vortex.

Although the data are considerably scattering among the systems, the global tendency of St~Re curve of System VI, VII agree well with that of other larger systems in air flow [14], except the sudden fall of St at Re around $1.5\times10^4 \sim 2.2\times10^4$. In the range of $10^3 < \mathrm{Re} < 3.5\times10^3$, the Strouhal number increases with a significant gradient from 0.02 to 0.04, but the value of St seems considerably larger for System VII. In the range of $3.5\times10^3 < \mathrm{Re} < 10^5$, Strouhal number for systems tested in the wind tunnel decreases very gradually. While in the cases of systems VI, VII tested in the water tunnel Strouhal number agrees well with that in air flow when $\mathrm{Re}<1.5\times10^4$, but it begins to fall down suddenly at $\mathrm{Re}=1.5\times10^4$ and becomes nearly to zero at $\mathrm{Re}\sim2.2\times10^4$. This phenomenon is corresponding with the fact that the peaks in the velocity spectra S_u became lower and finally vanished as seen in Fig.4. The results in Fig.7 (b) show that the characteristics of the necklace vortex shedding are universal in the Reynolds number region of $10^3 < \mathrm{Re} < 1.5\times10^4$ for various cylinder sizes in both water and air flow. The peculiar behavior of St~ Re curve at $\mathrm{Re} > 1.5\times10^4$ for the necklace vortex obtained in water tunnel B will be discussed at the end of this chapter.

3.4 Fluctuating lift force loading on the upstream cylinder

Figures 8 (a), (b), (c) present the spectra of the velocity and the fluctuating lift force loading on the upstream cylinder for System VI in the cases of the trailing vortex, the necklace vortex and the vanishing of the necklace vortex, respectively. In Figs.8 (a) and (b) a sharp peak in the fluctuating lift force spectrum appears at a frequency coinciding with the frequency which was observed by the peak in the respective velocity spectrum. The second highest peak in S_L at a higher frequency in Fig.8 (b) is caused by the Karman vortex. In contrast, only the sharp peak due to Karman vortex at the frequency about 60 Hz is observed in Fig. 8 (c), but no peak for the necklace vortex appears both in S_u and S_L.

Figure 9 presents the relationships between the fluctuating lift coefficient C_{Lrms} and St obtained from S_L plotted against Reynolds number Re for System I and VI in both cases of the longitudinal vortices. Here, the fluctuating lift coefficient C_{Lrms} is defined by $C_{Lrms}=F_{Lrms}/0.5\rho U^2 dL_v$ as in the earlier paper [8], where F_{Lrms} is the root-mean-square of measured fluctuating lift loading on the upstream cylinder, L_v is the span wise length of the

vortex region. The same equations as in the earlier paper [8] are used to estimate L_v: L_v= 6.2d in the case of the trailing vortex and 5.2d in the case of the necklace vortex. In Figs. 9(a) and (b), agreement of St ~ Re between the two systems is excellent except the peculiar behavior of St for the necklace vortex shedding at Re>1.5×10^4 just the same as observed in Fig.7 (b). While, agreement of the lift coefficient is only fair for the both longitudinal vortices. For System VI, C_{Lrms} of the trailing vortex remains constant at around 0.22 over the range of Reynolds number from 10^4 to 4×10^4. This result seems more plausible than the data for System I since the latter decreases steeply with Re. While the C_{Lrms} of the necklace vortex for System I in Fig. 9(b) is about 0.4 over the range of Re from 5×10^3 to 3×10^4, for System VI it decreases gradually from 0.4 to 0.25 when 5×10^3 <Re< 1.5×10^4, keeps a constant value about 0.25 in the transition region 1.5×10^4 <Re< 2.2×10^4 and increases gradually to 0.4 in the higher Re region from 2.2×10^4 to 3.5×10^4. It is noted that the necklace vortex disappears in this high Re region as mentioned above. Results as given Figs. 8 and 9 show that the behavior of the lift force loading on the upstream cylinder correlate well with those obtained from velocity measurement for the cases of the trailing vortex and the necklace vortex.

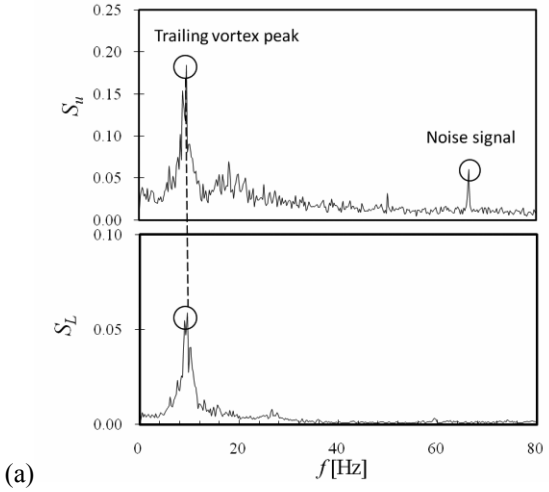

(a)

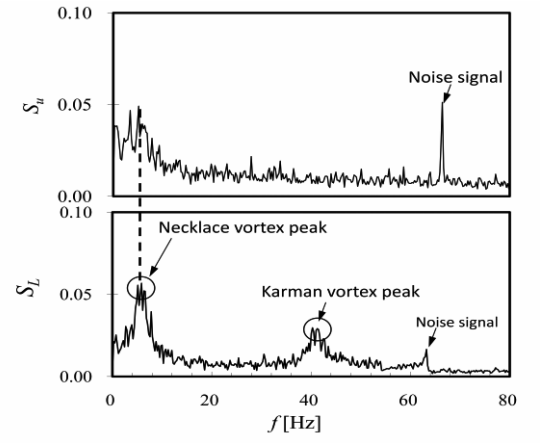

(b)

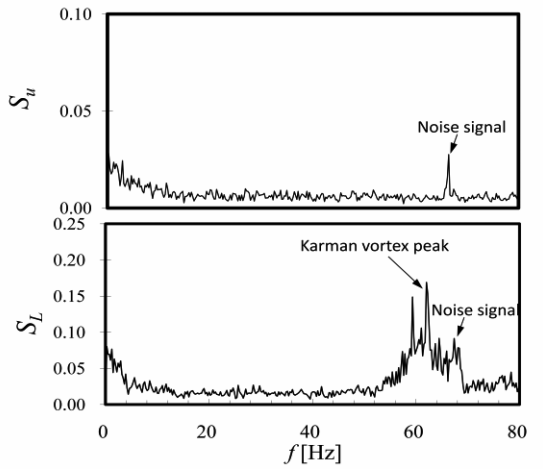

(c)

Fig. 8 S_L and S_u for System VI. (a) Trailing vortex (s/d=0.08, U=1.3 m/s); (b) Necklace vortex (s/d=0.3, U=1.9 m/s); (c) Vanishing of the necklace vortex (s/d=0.3, U=2.8 m/s).

Based on the dynamic similarity theory, the peculiar behavior of the necklace vortex in the high Re region observed in Water Tunnel B can be attributed to the slight defects of geometrical similarity and difference in characteristics of the approaching flow.

From the former, the aspect ratio is excluded from the causes by the similar reasoning as given earlier for Fig.7. Since the end plates are not strictly geometrically similar, an experiment with a system in which the end plates of System VI were removed and the upstream cylinder was fixed directly to the side walls of the measuring section was

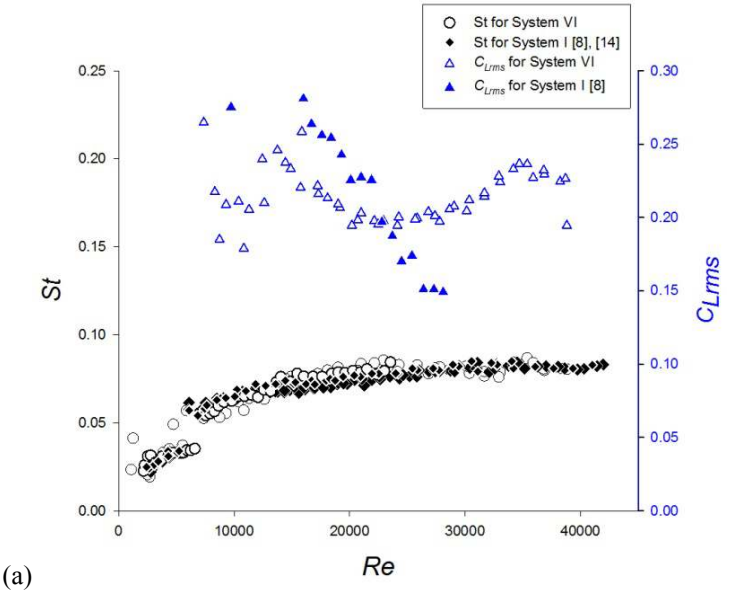

(a)

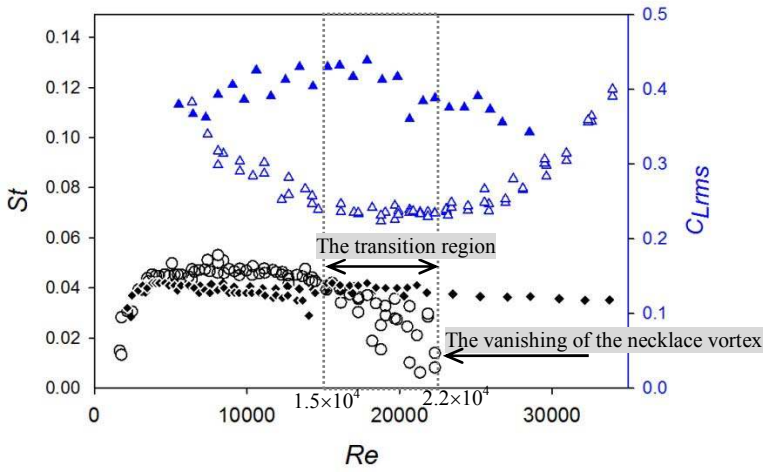

(b)

Fig.9 The relationship between the fluctuating lift coefficient C_{Lrms} and Reynolds number Re for System I and VI. (a) s/d= 0.08; (b) s/d=0.28 for System I and 0.3 for System VI.

conducted. Since almost the same results as given in Figs.4 (b) and 7 (b) were obtained in this experiment, the effect of end plates is also excluded. Therefore, the potential causes remaining at present are the differences in uniformity and turbulence of approaching flow.

4. Conclusion

In this study, universality of the two longitudinal vortices shedding from a cruciform two cylinder system is investigated by carrying out experiments in water and wind tunnels over the range of Reynolds number 10^3<Re<4×10^4 comparable with data for the various larger size systems in air flow obtained in the earlier studies [8], [14]. The aspect ratios of the systems tested in this study are little lower or higher than those in the earlier works covering a range of 7<A_R<14. Measurements of velocity and lift in the water tunnel confirm that the longitudinal vortices shed periodically and generate alternating lift force exerting on the upstream cylinder over different ranges of Reynolds number: 10^3<Re<4×10^4 for the trailing vortex and 10^3<Re<1.5×10^4 for the necklace vortex.

The vortex regime transits abruptly at s/d= 0.25~0.28, i.e. the trailing vortex sheds when s/d≤0.25~0.28 and the necklace vortex sheds when 0.25~0.28 ≤ s/d ≤ 0.5. The results

of the velocity spectrum peaks show that the vortices shed most regularly at $s/d<0.08$ for the trailing vortex, and at $0.28<s/d<0.32$ for the necklace vortex.

The relationship between St, C_{Lrms} and Re for various size systems in both air and water flow are fairly consistent over a wide range of Re number except the peculiar vanishing of the necklace vortex when Re is higher than about 2.2×10^4 in the small water tunnel.

The alternating lift force loads on the upstream cylinder at a same frequency of the vortex shedding for both cases of longitudinal vortices.

For the systems in the largest wind tunnel, the experimental results show some discrepancies from the others such as: the transition point between the two vortices shifts to 0.28, the vortex shedding frequency shifts to 30 ~ 50 % lower. The causes of these phenomena and the vanishing of the necklace vortex at the high Re region in the smaller-size water tunnel are left to be clarified in the near future.

References

[1] Blevins, R. D., *Flow-Induced Vibration*, Van Nostrand Reinhold, (1990) New York.

[2] Bearman, P.W., Vortex shedding from oscillating bluff bodies, *Annual Revision of Fluid Mechanics*, Vol.16 (1984), pp. 195-222.

[3] Sarpkaya, T., A critical review of the intrinsic nature of vortex-induced vibrations, *Journal of Fluids and Structures*, Vol.19 (2004), pp.389-447.

[4] Khalak, A., and Williamson, C.H.K., Motions, forces and mode transitions in vortex-induced vibrations at low mass-damping, *Journal of Fluids Structures*, Vol.13 (1999), pp. 813-815.

[5] Govardhan, R., and Williamson, C.H.K., Modes of vortex formation and frequency response of a freely vibrating cylinder, *Journal of Fluid Mechanics*, Vol.420 (2000), pp. 85-130.

[6] Bae, H.M., Baranyi, L., Koide, M., Takahashi, T., and Shirakashi, M., Suppression of Karman vortex excitation of a circular cylinder by a second cylinder set downstream in cruciform arrangement, *Journal of Computational and Applied Mechanics,* Vol.2, No.2 (2001), pp.175-188.

[7] Shirakashi, M., Bae, H.M., Sano, M., Takahashi, T., Characteristics of periodic vortex shedding from two cylinders in cruciform arrangement, *Journal of Fluids Structures*, Vol.8, No.3(1994-3), pp. 239-256.

[8] Shirakashi, M., Takahashi, T., Kumagai, I., and Matsumoto, T., Vortex-induced vibration of the upstream cylinder of a two-cylinder system in cruciform arrangement, *Journal of Computational and Applied Mechanics*, Vol.2, No.1(2001), pp.103-122.

[9] Takahashi, T., Baranyi, L., Shirakashi, M., Configuration and frequency of longitudinal vortices shedding from two circular cylinders in cruciform arrangement, *Journal of the Visualization Society of Japan,* Vol.19, No.75 (1999), pp. 328-336.

[10] Zdravkovich, M. M., Interference between two circular cylinders forming a cross, *Journal of Fluid Mechanics*, Vol.128 (1983), pp.231-246.

[11] Fox, T.A., Flow visualization at the center of a cross composed tubes, *International Journal of Heat and Fluid Flow*, Vol.11, No.2 (1990), pp.160-162.

[12] Fox, T.A., Interference in the wake of two square-section cylinders arranged perpendicular to each other, *Journal of Wind Engineerng and Industrial Aerodynamics*, Vol.40, No1 (1992), pp. 75-92.

[13] Deng, J., Ren, A.-L., Shao, X.-M., The flow between a stationary cylinder and a downstream elastic cylinder in cruciform arrangement, *Journal of Fluids Structures*, Vol.23 (2007), pp. 715-731.

[14] Koide, M., Oogane, K., Takahashi, T., and Shirakashi, M., Experimental study on universality of longitudinal vortices shedding periodically from crisscross circular cylinder system (in Japanese), Journal of Visualization Society of Japan, Vol.24, No.4 (2004-4),

pp15-22.
[15] Koide, M., Ootani, K., Yamada, S., Takahashi, T., and Shirakashi, M., Vortex excitation caused by longitudinal vortices shedding from cruciform cylinder system in water flow, *JSME International Journal,* Series B, Vol.49, No.4 (2006), pp. 1043-1048.
[16] Shirakashi, M., Ishida, Y., and Wakiya, S., Higher velocity resonance of circular cylinder in cross flow, *Transaction of the ASME, Journal of Fluids Engineering*, Vol.107 (1986), pp.392 -396.
[17] Koide M., Takahashi T. and Shirakashi M., Development of a ring-type vortex anemometer for low-velocity wind tunnel experiments, *Bulletin of Japan Society of Mechanical Engineering,* (in Japanese), Vol.67, No657, B(2001), pp.1105-1111.